ACS APPLIED MATERIALS & INTERFACES

Research Article

www.acsami.org

Fabrication of Si/ZnS Radial Nanowire Heterojunction Arrays for White Light Emitting Devices on Si Substrates

Ajit K. Katiyar, Arun Kumar Sinha, Santanu Manna, and Samit K. Ray*

Department of Physics, Indian Institute of Technology, Kharagpur, West Bengal 721302, India

Supporting Information

ABSTRACT: Well-separated Si/ZnS radial nanowire heterojunction-based light-emitting devices have been fabricated on large-area substrates by depositing n-ZnS film on p-type nanoporous Si nanowire templates. Vertically oriented porous Si nanowires on p-Si substrates have been grown by metal-assisted chemical etching catalyzed using Au nanoparticles. Isolated Si nanowires with needle-shaped arrays have been made by KOH treatment before ZnS deposition. Electrically driven efficient white light emission from radial heterojunction arrays has been achieved under a low forward bias condition. The observed white light emission is attributed to blue and green emission from the defect-related radiative transition of ZnS and Si/ZnS interface, respectively, while the red arises from the porous surface of the Si nanowire core. The observed white light emission from the Si/ZnS nanowire heterojunction could open up the new possibility to integrate Si-based optical sources on a large scale.

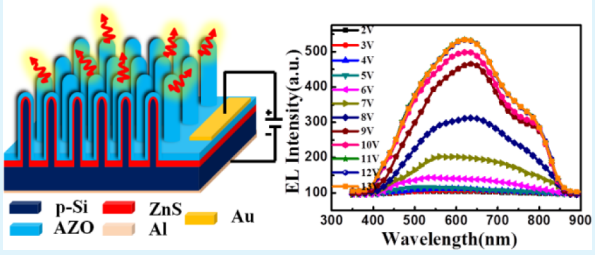

KEYWORDS: *metal-assisted chemical etching, Si nanowires, Si/ZnS heterojunction, nanowire heterojunction, electroluminescence, white light emission*

INTRODUCTION

Silicon has dominated years of success in the microelectronic industries[1−3] with relatively slow progress for photonic devices. Numbers of silicon-based optical devices, such as optical modulators and photodetectors, have been developed for the realization of photonic integrated circuits. However, the fabrication of efficient silicon-based light-emitting devices is one of the challenging goals, since bulk Si is an indirect band gap semiconductor and consequently exhibits poor near-infrared (NIR) light emission. Following the discovery of light emission in the visible spectrum from porous silicon,[4] significant efforts have been made to develop new silicon nanostructures to realize efficient light emitters. Various nanostructures of Si such as quantum dots,[5] porous silicon,[6,7] and Si nanowires[8−10] have been explored to fabricate homojunction- or heterojunction-based light-emitting devices (LED). In fabrication of heterojunctions, a large lattice mismatch between two semiconductors in a heterojunction leads to the formation of defects and dislocations, which affect the performance of resultant devices. So an appropriate material combination with negligible lattice mismatch is highly desirable for fabricating efficient heterojunction devices.

Zinc sulfide (ZnS), a II−VI compound semiconductor, is attractive for its direct wide band gap (~3.68 eV) at room temperature with large excitonic binding energy (40 meV), excellent transport properties, good thermal stability, and high electronic mobility. These properties make ZnS one of the most potential semiconductors for optoelectronics with a variety of applications including n-window layers for solar cells,[11] blue light emitting diodes,[12,13] electroluminescent displays,[14] photoluminescence devices,[15] etc. Moreover, ZnS is lattice matched with Si (mismatch ~0.2%), which makes it attractive for the integration of optoelectronic devices with Si.[16] Therefore, the ZnS/Si heterojunction possesses the combined merits of the optoelectronic properties of ZnS and Si based planar device technology.

Solid-state white light emitting devices have wide applications in color display, backlight for liquid crystal display, and broad-band sources. Commonly, white light is produced by combining the emission from three LEDs (red, green, and blue) or by coating phosphors on blue indium gallium nitride (InGaN) LED chips. In recent years, several studies have been reported on Si/ZnS nanoheterostructures showing strong visible photoluminescence ranging from blue to red at room temperature,[17−19] indicating their potential in solid-state white light emitting devices. However, electrically driven light emitters using Si/ZnS heterojunctions are essential for application in LED devices. In the present paper, we propose a new approach to fabricate well-separated large-area Si/ZnS nanowire heterojunction arrays without using any sophisticated lithography technique. The fabricated vertically aligned radial heterojunction arrays using a bottom-up approach provide significantly larger active areas, with an improved carrier transport and enhanced light emission as compared to the thin-film heterostructures.

Received: May 12, 2014
Accepted: August 19, 2014
Published: August 19, 2014

EXPERIMENTAL SECTION

Highly ordered vertically aligned Si nanowire arrays (SiNWs) on planar silicon substrates were prepared by metal-assisted chemical etching (MACE) using Au nanoparticles as a catalyst. The fabrication method has been reported in detail elsewhere.[20] In brief, boron-doped p-type single side polished Si (100) substrates with a resistivity of 2–10 Ω·cm were first cleaned through the standard RCA cleaning process. Thereafter, the cleaned H-terminated Si pieces were placed into a gold coating solution containing 4.8 M HF and 0.005 M $HAuCl_4$ for 1 min, resulting in a uniform layer of Au nanoparticles (Au NPs) on Si. The Au NPs coated Si wafer was then immersed in an etchant solution containing 4.8 M HF and 0.4 M H_2O_2 for 20 min resulting in the formation of a dense nanowires array. On completion of the etching process, residual gold was dissolved by putting the nanowire templates in a dilute aqua regia (HNO_3/HCl/H_2O 1:3:2) solution. To decrease the areal density and to separate their top ends, as-fabricated Si nanowire templates were kept in 10 wt % aqueous KOH solution at room temperature for 120 s. Following KOH etching, the wafers were washed with 2% HF to remove the native oxide layer, cleaned with DI water for several times, and dried under N_2 flow.

To fabricate p-Si/n-ZnS radial heterojunctions, ZnS film was deposited on KOH-treated Si nanowire templates by a pulsed laser deposition (PLD) technique from a high-purity (99.999%) ZnS target. Si nanowire templates (1 × 1 cm^2) were placed at a distance of 10 cm from the ZnS target. The target was ablated using a KrF excimer laser (λ = 248 nm, τ = 25 ns) at an energy density of ∼2 J/cm^2 with the repetition rate of 5 Hz. During deposition, the temperature of the substrate was maintained at 200 °C and the typical pressure inside the chamber was ∼10^{-7} Torr. To complete the device fabrication, nearly 20 nm of transparent and conducting Al-doped ZnO (AZO) film was deposited by PLD. The 20 nm thick AZO film grown under an optimized condition (pressure ∼5 × 10^{-6} Torr, substrate temperature ∼300 °C, and laser fluence ∼2 J/cm^2) exhibits resistivity of ∼7.2 × 10^{-4} Ω·cm and an average transmittance of ∼92% in the visible wavelength range (see Figure S1 of the Supporting Information). A thick aluminum layer was deposited by thermal evaporation onto the backside of the devices to form the bottom ohmic contact.

Surface morphology and crystalline quality of Si/ZnS heterostructures were studied by field emission scanning electron microscopy (FESEM) using a ZEISS SUPRA 40 microscope and transmission electron microscopy (TEM) using a JEOL JEM-2100F microscope. The phase of nanowire heterojunctions was studied by X-ray diffraction (XRD) (Philips X-Pert MRD) at a grazing incidence mode using Cu Kα radiation (45 kV, 40 mA). The chemical states of ZnS/SiNWs heterostructures were studied by X-ray photoelectron spectroscopy (XPS) using PHI 5000 Versa Probe II (ULVAC, PHI, Inc., Japan) system equipped with a microfocused (100 μm, 25 W, 15 kV) monochromatic Al Kα X-ray source of energy 1486.6 eV. Temperature- and bias-dependent electroluminescence measurements were carried out using a TRIAX-320 monochromator and Hamamatsu R928 photomultiplier detector in the visible range. Photoluminescence spectra were also recorded with the same monochromator and detector combination using a He–Cd laser as the excitation source operating at 325 nm with an output power of 40 mW. The current–voltage (I–V) characteristics of the heterojunctions were studied using a Keithley semiconductor parameter analyzer (model no. 4200-SCS).

RESULTS AND DISCUSSION

A few recent reports[20,21] have indicated that nanowires fabricated through the MACE technique using Au nanoparticles possess uniform porosity than those using Ag nanoparticles as catalysts. Therefore, in the present work, we have chosen Au nanoparticles as catalysts to obtain improved photoluminescence (PL) and electroluminescence (EL) characteristics. A typical FESEM image of as-synthesized nanowires on p-Si substrate is shown in Figure 1a. Highly dense, vertically oriented Si nanowires of nearly 5.0 μm length with a diameter

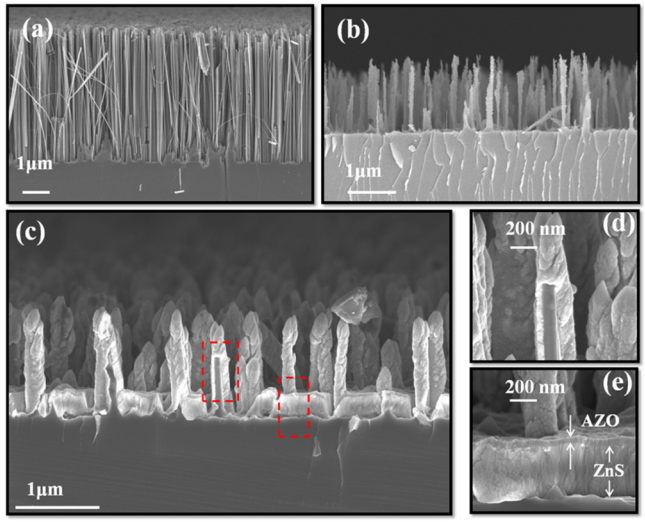

Figure 1. FESEM images of (a) Si nanowire fabricated through MACE using Au nanoparticles as catalyst. (b) Si nanowire after KOH treatment. (c) Fabricated well-separated radial heterojunction arrays by depositing ZnS and AZO on KOH-treated nanowires. (d) Cross-sectional image of a single device showing the Si core and ZnS shell. (e) Bottom part of the radial heterojunction showing ∼50 nm AZO and ∼400 nm ZnS films.

ranging from 30 to 200 nm are observed. Si nanowires fabricated through the MACE technique have the tendency of agglomeration with the bundling of their top ends due to van der Waals force.[22] It is necessary to separate the nanowire tips to fabricate heterojunction devices with material deposited through a physical vapor technique. Therefore, to fabricate SiNWs/ZnS radial heterojunctions through PLD, we have used the anisotropic etching behavior of crystalline Si in a potassium hydroxide (KOH) solution to separate the nanowires tips by sharpening their top ends.[23] The FESEM micrographs of Si nanowires etched with KOH (10%) as a function of etching time are shown in Figure S2 of the Supporting Information. By optimizing the concentration of KOH and etching time, we have fabricated well-separated nanowires having length of nearly 2 μm with an average diameter of ∼100 nm, as shown in the micrograph Figure 1b. The needle-like sharp-tipped nanowires are formed due to the faster etching rate at the corner edges than the flat regions of nanowires,[23,24] though the average length of the nanowire is reduced from 5 to 2 μm. This needle-shaped structure can be extremely useful to exhibit efficient electroluminescence, because of the generation of a stronger electric field at the tip using a low external bias. Figure 1c shows the typical FESEM image of a SiNWs/ZnS/AZO heterojunction array. The average diameter of the SiNWs/ZnS/AZO core–shell structure is found to be ∼300 nm. It is clear that even after the deposition of ZnS and AZO, nanowires are still well-separated, and thus each of them can act as an individual nano-LED device under proper biasing condition. The deposition profile on nanowires and the spacing between them (area between the bases of nanowires) are found to be different. Parts d and e of Figure 1 present the magnified images of a single radial heterojunction and it is bottom portion, respectively, in the region highlighted by red squares in Figure 1c. The thickness of ZnS film on the nanowire and the substrate is found to be different. The thickness of deposited films of ZnS and AZO on the substrate is ∼400 and ∼50 nm, respectively. The thickness of the deposited ZnS and AZO

layers on either side of the Si nanowire is found to be slightly different due to the step coverage problem of the PLD process with a highly directional plume. This problem can be overcome using a suitable chemical vapor deposition process for ZnS and AZO layers. Since the thickness of ZnS and AZO is not clearly distinguished in FESEM micrographs, TEM images of Si nanowire and SiNWs/ZnS/AZO radial heterojunction are analyzed in Figure 2.

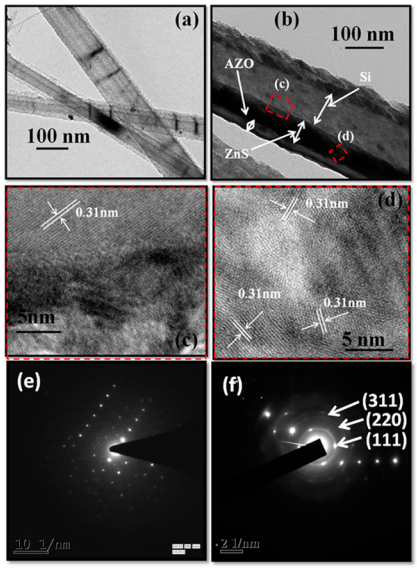

Figure 2. TEM images of (a) KOH-treated Si nanowire. (b) SiNW/ZnS/AZO core–shell heterostructure showing ~100 nm Si core, ~80 nm ZnS, and ~20 nm thick AZO layers (the portion highlighted by red squares and labeled as c and d are magnified in panels c and d, respectively). (c) Magnified HRTEM image of the Si/ZnS interface showing the single-crystalline Si core. (d) HRTEM image of the polycrystalline ZnS shell. (e) SAED pattern from the Si nanowire core. (f) SAED pattern from the Si/ZnS core–shell structure.

Figure 2a reveals that the nearly 100 nm crystalline Si core is surrounded by ~20 nm porous Si. It is clear from Figure 2b that the fabricated Si/ZnS/AZO radial heterojunction contains ~80 nm ZnS and ~20 nm thick AZO layers, which are much lower than those deposited on the substrate. High-resolution TEM images of the Si/ZnS interface and ZnS shell (labeled by red squares as c and d in Figure 2b) reflect the crystalline quality of the Si core and ZnS shell, which are shown in Figure 2, parts c and d, respectively. The results demonstrate that the Si core is single-crystalline in nature, while the surrounding ZnS shell is polycrystalline. The measured lattice fringes spacing for Si core is 0.31 nm, which is in agreement with that of the (111) plane of silicon. Lattice spacing of the several grains of polycrystalline ZnS shell is also found to be 0.31 nm, which is typical for the (111) *d*-spacing of zinc blende ZnS. Parts e and f of Figure 2 present the selected area electron diffraction (SAED) patterns of an individual Si nanowire and Si/ZnS core–shell structure, respectively. SAED pattern of the Si core indicates the formation of crystalline nanowire, as shown in Figure 2e. On the other hand, the Si/ZnS core–shell structure exhibits the diffraction rings owing to (111), (220), and (311) planes of zinc blende ZnS on the background of Si diffraction spots in Figure 2f. The HRTEM results are consistent with the XRD data shown in Figure 3a. In the XRD pattern the diffraction peaks observed at 2θ = 28.6°, 47.6°, and 56.5°, are labeled using the JCPDS card (file no. 41–1049) and are attributed to (111), (220), and (311) crystallographic planes of zinc blende ZnS. In addition a strong (004) peak from the Si nanowire core is also observed, indicating the formation of crystalline ZnS/Si heterojunctions.

To study the chemical composition and bonding of deposited films and interfaces, XPS measurements have been carried out. High-resolution core-level spectra of Zn 2p and S 2p electrons are shown in Figure 3b. Two strong peaks for Zn 2p electrons observed at 1022.3 and 1045.2 eV are assigned to $2p_{3/2}$ and $2p_{1/2}$ levels, respectively. The binding energy spectrum observed for S 2p electrons is deconvoluted into two Gaussian peaks located at 162.3 and 163.6 eV, attributed to the S $2p_{3/2}$ and S $2p_{1/2}$ states, respectively. The observed peak positions of spin–orbit doublets of Zn 2p and S 2p electrons, which are in excellent agreement with literature,[25] confirm the presence of pure ZnS shell in the as-fabricated core–shell structure. However, the atomic percentage ratio for Zn and S, extracted using sensitivity factor and area under the curve of Zn 2p and S 2p peaks using Shirley background correction, is found to be 52:48. This clearly indicates the abundance of Zn atoms and existence of sulfur vacancy, which may strongly influence the emission characteristics of Si/ZnS heterojunctions. Since the presence of a native oxide can strongly influence the carrier transport across the junction in Si-based heterojunction devices,[26] XPS analysis has also been used to probe the Si/ZnS interface. For this, we performed XPS depth profile analysis by sputter-etching the outer ZnS layer with 2.0 keV Ar^+ ions until the signal from the Si core is detected. The typical XPS spectrum of Si 2p originated from Si/ZnS interface is presented in Figure 3c. The spectrum can be resolved into three Gaussian peaks located at 99.6, 101.5, and 103.6 eV, corresponding to the chemical state for Si, SiO_x ($1 < x < 2$), and SiO_2, respectively. The oxygen signal (O 1s) is detected only at the Si/ZnS interface, as shown in Figure 3d. The O 1s spectrum for Si/ZnS interface is deconvoluted into two Gaussian peaks. Two distinguishable peaks appear at 532.9 and 531.6 eV due to lattice oxygen in SiO_2 and adsorbed hydrocarbon contamination, respectively. This indicates the formation of a thin SiO_2 layer at the interface, which may affect the electrical property of the heterojunction device.

The fabricated Si/ZnS/AZO radial heterojunction device is schematically illustrated in Figure 4a. Since undoped ZnS film exhibits n-type conductivity with a carrier concentration of ~10^{16}/cm^3,[19] the deposition of ZnS on p-Si nanowire leads to the formation of a core–shell-type, radial p–n heterojunction. In order to compare the electrical transport and optical characteristics of a SiNWs/ZnS radial heterojunction with the planar one, a planar thin-film heterojunction has also been fabricated. Figure 4b shows the room-temperature current density–voltage (J–V) characteristics under dark for SiNWs/ZnS and planar Si/ZnS heterojunctions. The forward current density of the nanowire and planar junction is found to be ~9.9 and ~2.3 mA cm^{-2}, while the leakage current density is observed as ~0.006 and ~0.09 mA cm^{-2}, respectively, for ±3 V bias. The rectification ratio is found to be approximately 1651 and 24 at a bias voltage of ±3 V for SiNWs/ZnS and planar Si/ZnS, respectively. Thus, the rectifying behavior of the nanowire radial heterojunction is much superior to that of the planar device. The current density (J) versus voltage (V) characteristics of a real diode can be expressed using the Richardson–Schottky diode equation:

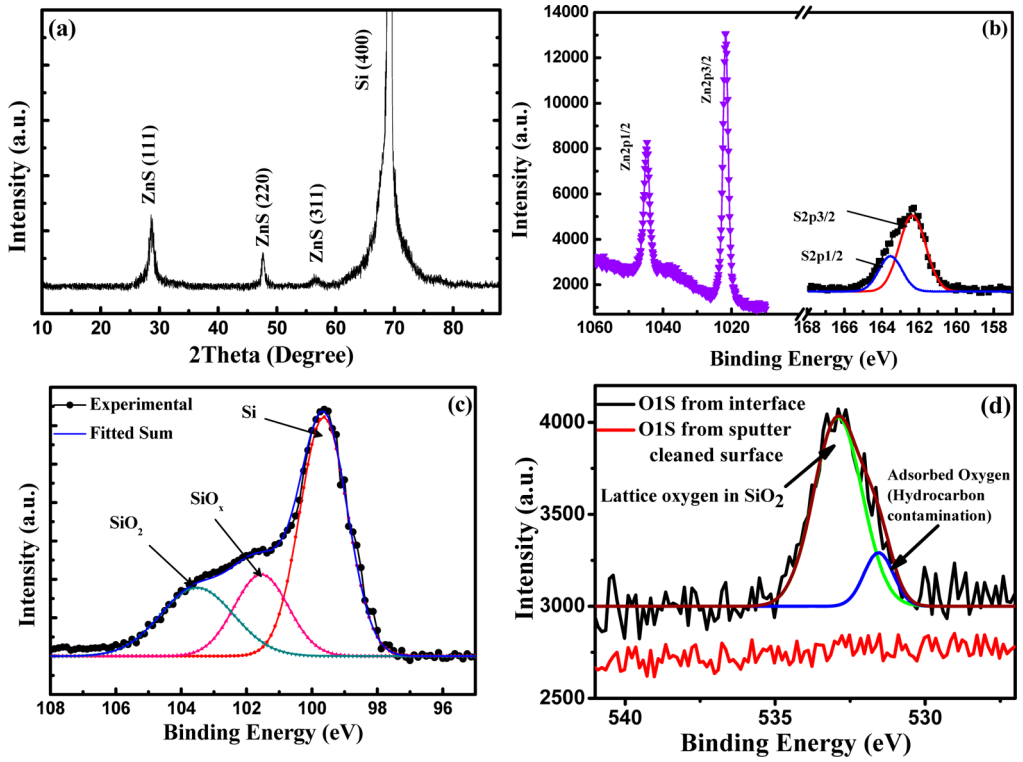

Figure 3. (a) XRD spectra of core−shell radial heterojunction arrays. The spectrum was recorded at 2° grazing incidence angle. (b) High-resolution XPS spectra for Zn 2p and S 2p core-level electrons from a sputter-cleaned surface of the radial heterojunction arrays. (c) XPS spectrum of Si 2p electrons originating from the Si/ZnS interface. (d) O 1s spectra for a sputter-cleaned surface and Si/ZnS interface.

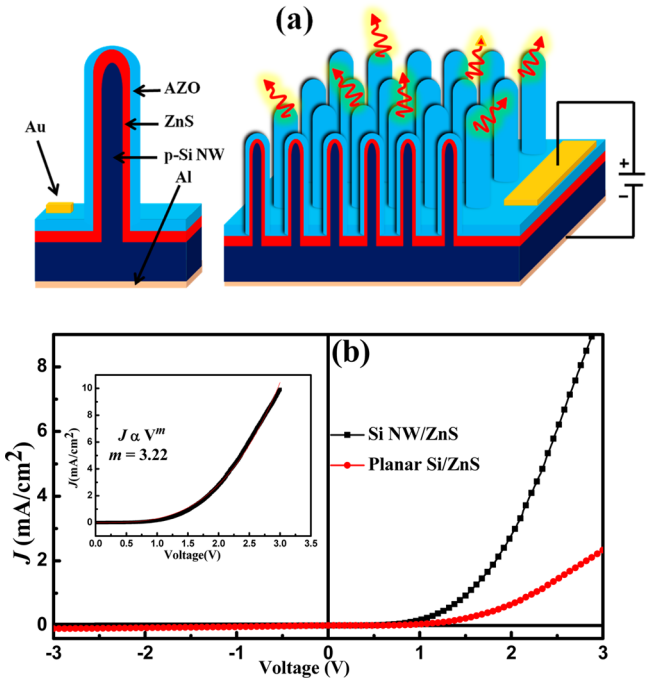

Figure 4. (a) Schematic diagram illustrating coaxial SiNW/ZnS/AZO radial heterojunctions for electroluminescent device. (b) J−V characteristics of fabricated SiNWs/ZnS core−shell-type radial and planar heterojunctions under dark, at room temperature. The inset shows the fitted J−V curve for the radial heterojunction following a power law $J \propto V^m$ corresponding to the trap-charge-limited current transport.

$$J = J_0\left\{\exp\left[\frac{q(V - IR_s}{\eta KT}\right] - 1\right\} \quad (1)$$

where J_0 is the reverse saturation current density, I is current, R_s is series resistance, and "η" is the ideality factor of the diode. The ideality factor can be calculated using the equation

$$\eta = \frac{q}{kT}\frac{\partial V}{\partial \ln J} \quad (2)$$

The higher forward current density of the nanowire heterojunction over the planar one could be explained using eq 1. Calculated values of "η" from eq 2 are found to be ∼6.6 and ∼11.3 for the SiNWs/ZnS and planar junction, respectively. The values signify the nonideal behavior of both the heterojunctions. This is probably due to the presence of high density of interface states at SiNWs/ZnS and/or the presence of an insulating SiO_2 layer at the interface. In the case of the nanowire heterojunction, the observed reverse saturation current density (J_0) is only 0.006 mA cm^{-2} at a reverse bias of 3 V, which is fairly small in comparison to 0.09 mA cm^{-2} for the planar one. The diode ideality factor of the present Si/ZnS nanowire radial heterojunction is superior to that reported for a similar structure fabricated with Si nanoporous pillar arrays (η ∼ 29.6).[19] However, the forward current density for our device is lower compared to that reported (75 mA/cm^2) in the above study. This may be due to relatively higher contact resistance of the AZO electrode compared to a pure metal electrode. The comparison of electrical performance of different Si/ZnS heterojunctions reported in literature is presented in Table 1. The results indicate the superior electrical performance in terms of diode ideality factor and rectification ratio for the Si/ZnS nanowire heterojunctions. The J−V curve of the SiNWs/

Table 1. Comparison of Electrical Performance of Different Si/ZnS Heterojunctions Reported in Literature

device structure	forward current density (mA/cm^2)	rectification ratio	diode ideality factor	ref
Si NW/ZnS radial heterostructure	9.9 @ 3 V	1651 @ ± 3 V	6.6	this work
Si nanoporous pillar/ZnS heterostructure	75 @ 2 V		29.6	19
porous Si/ZnS heterostructure		520 @ ± 7.5 V	77	35
crystalline Si/ZnS heterostructure		7000 @ ± 4 V	7	36

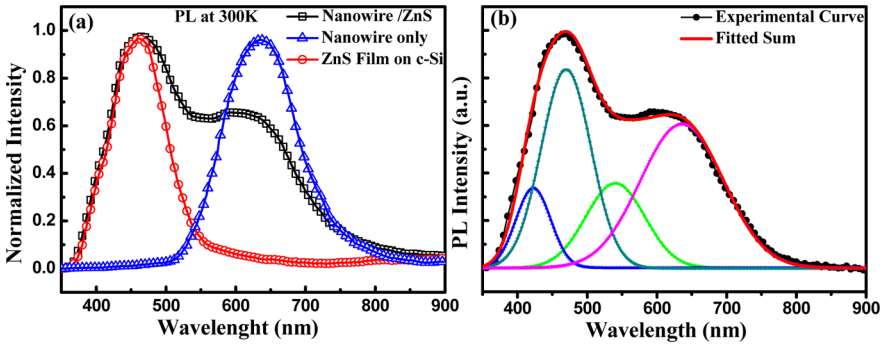

Figure 5. (a) Normalized room-temperature PL spectra of ZnS film on c-Si, KOH-treated porous Si nanowire, and SiNWs/ZnS radial heterojunction arrays. (b) Deconvoluted room-temperature PL spectrum of SiNWs/ZnS radial heterojunction arrays.

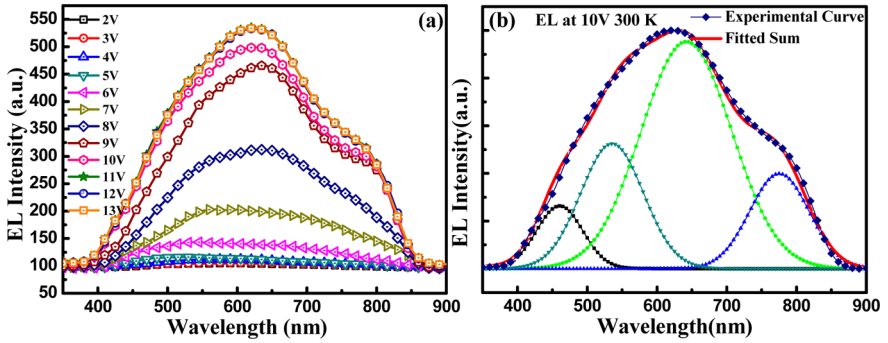

Figure 6. (a) Room-temperature electroluminescence spectra of SiNWs/ZnS radial heterojunction arrays under different forward bias. (b) Deconvoluted EL spectrum of SiNWs/ZnS radial heterojunction arrays under 10 V forward bias at room temperature.

ZnS radial heterojunction is best fitted by the equation $J \propto V^m$, with the exponent $m = 2.33$ and the proportionality constant as 0.001, which is shown in the inset of Figure 4. So the charge transport of nanowire heterojunction could be explained by the trap-charge-limited current (TCLC) model.

The origin of the electroluminescence (EL) emission in radial heterojunction diodes can be explained by studying their photoluminescence (PL) spectra. The normalized PL spectra of the ZnS films, porous Si nanowires, and SiNWs/ZnS radial heterojunction arrays, recorded at room temperature, are shown in Figure 5a. Under excitation by 325 nm pump, the PL emission of the Si/ZnS radial heterojunction covers the visible spectrum from ~400 to ~800 nm and the contribution from both porous Si nanowires and ZnS film is clearly evident. The experimentally obtained PL spectrum of the radial heterojunction is deconvoluted into four Gaussian peaks centered at 422, 463, 540, and 636 nm, as shown in Figure 5b. The first two peaks are attributed to sulfur vacancy and interstitial sulfur lattice defects in ZnS.[27,28] The emission band centered around 636 nm is considered to be originated from the porous Si nanowire core beneath the outer ZnS shell, as the peak position and full width at half-maximum (fwhm) agree well with the emission from the Si nanowire shown in Figure 5a. The emission with similar energy has also been reported for porous Si NWs in previous studies by different groups.[29,30] The observed green emission band centered at ~540 nm with a fwhm ~95 nm can be related to SiNWs/ZnS heterojunction, because this emission band is observed only in nanowire heterostructure.

The novelty of fabricated Si/ZnS radial heterojunction arrays is the realization of broad-band EL emission using a low applied voltage at and above the room temperature. A white light emission could be directly observed by the naked eye when sufficient forward bias is applied across the device with AZO as the cathode and Al as the anode. The EL spectra of ZnS/Si radial heterojunction arrays at different applied bias in the range of 2−13 V are shown in Figure 6a. A broad emission band starting from 400 nm, covering the full visible region and extended to the NIR region (850 nm), can be observed. The EL intensity increases with the increase of injection of electrons across the junction, above a threshold bias ~4 V. To understand the origin of broad-band emission from SiNWs/ZnS radial heterojunction, the EL spectrum at room temperature for 10 V is fitted by Gaussian function, and the result is shown in Figure 6b. The spectrum consists of four distinct subbands centered at 460, 535, 640, and 775 nm with fwhm of about 73, 105, 155, and 100 nm, respectively. By comparing with the PL spectrum shown in Figure 5b, the emission band centered at around 460 nm is predicted to be due to the transition from the conduction band of ZnS to the interstitial

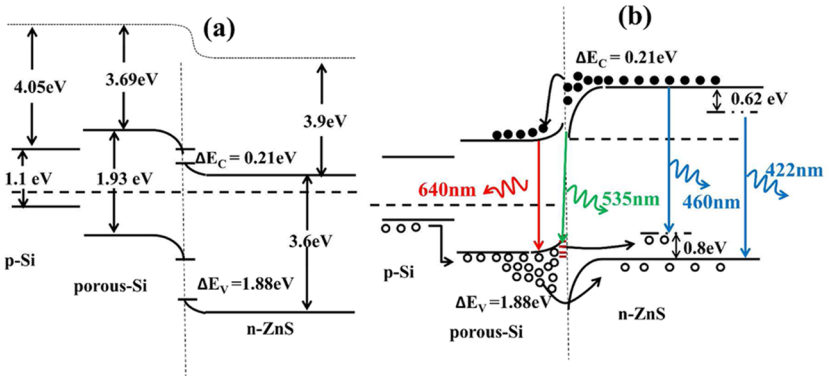

Figure 7. (a) Energy band diagram of the SiNWs/ZnS core−shell heterojunction under zero applied bias. (b) Energy band diagram demonstrating different transitions for EL emission under forward bias condition.

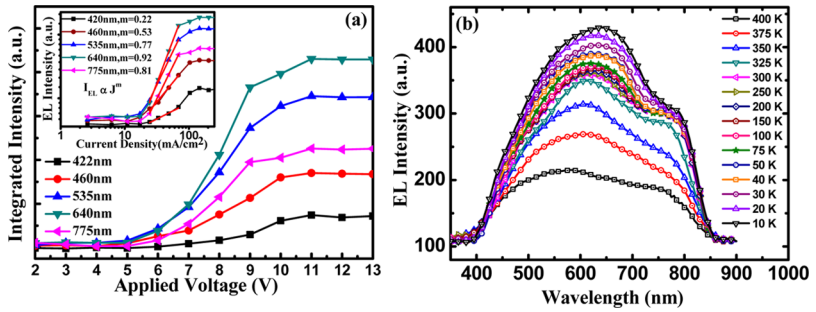

Figure 8. (a) Integrated intensity of different sub-bands as a function of forward bias. The inset shows the log−log plot of integrated intensity vs injected current density for different emission peaks. Solid red lines are the best-fitted linear portion, following the equation $I_{EL} \propto J^m$. (b) EL spectra of the nanowire heterojunction at different temperatures from 10 to 400 K under a forward bias of 10 V.

sulfur lattice defects. Theoretically, it has been reported that the position of interstitial sulfur defects level S_i is located 0.8 eV above the valence band of ZnS.[27] Thus, the emission energy of ∼460 nm (2.7 eV) agrees well with the transition from the conduction band of ZnS to this level. It may be noted that the emission band centered at around 422 nm observed in the PL spectrum (Figure 5b) is either very less intense or absent in the EL spectrum. This emission may arise due to the transition from the sulfur vacancy level to the valence band of ZnS. Sulfur vacancies in ZnS produce localized donor levels at an energy of ∼0.62 eV below the conduction band,[28] and thus the transition from this to the conduction band of ZnS results in the emission at ∼422 nm. The EL band centered at 640 nm agrees well with the position and fwhm of the PL spectra for porous Si nanowire (shown in Figure 5a). This reveals that EL and PL are attributed to the same carrier recombination mechanism in nanowire heterostructures. The green emission band centered at around 530 nm may originate due to the transition from the conduction band of ZnS to some self-activated centers, or vacancy states at the SiNWs/ZnS interface. The most noticeable difference between the PL and EL spectrum is the observation of an EL emission band centered at 775 nm, which is absent in the PL spectra. This may originate due to the injection of electrons across another heterojunction formed between Si substrate and ZnS film grown at the bottom of the Si nanowire (shown in the FESEM micrograph Figure 1e).

The mechanism of visible light emission through radiative recombination of charge carriers injected in the SiNWs/ZnS radial heterojunction could be explained using the proposed energy band diagram under zero and forward bias as shown in Figure 7, parts a and b, respectively. To draw the band diagram, we have taken the electron affinity of Si (χ_{Si}), porous Si(χ_{PSi}), and ZnS (χ_{ZnS}) as 4.05, 3.69,[31] and 3.9 eV,[32] respectively, while the band gap values are 1.12, 1.93, and 3.6 eV, respectively. Electron affinity and band gap values of c-Si and ZnS are taken from the literature, while the band gap of porous Si nanowires is determined from the PL measurement (see Figure S3 of Supporting Information). Neglecting the band bending at the c-Si/porous Si interface and the effect of the thin oxide layer at the Si/ZnS interface, the above parameters lead to a barrier for electrons as 0.21 eV (ΔE_C) and the barrier for holes as 1.88 eV (ΔE_V) at the SiNWs/ZnS interface. Obviously, a lower conduction band offset favors the efficient injection of electrons from ZnS into the porous Si nanowire side and a relatively high valence band offset assists the confinement of the holes in the ZnS−Si nanowire interface (Figure 7b). Hence, the emission from porous Si nanowire (640 nm) dominates over that from ZnS, which is clear from Figure 6b.

The integrated intensity of different emission peaks as a function of forward bias is shown in Figure 8a. The detectable emission of all transitions started around 4 V and increases continuously up to 9 V. Thereafter, the increasing trend of the EL intensity slows down gradually and saturates above 11 V. Similar emission behavior had already been observed in various heterojunction-based LEDs.[33,34] The behavior is attributed to the high Joule heating, or saturation of recombination centers at higher injection condition, affecting the performance of the device. The integrated EL intensity (I_{EL}) versus injected current density (J) characteristics is considered to obey a power law nature, $I_{EL} \propto J^m$, where the exponent "m" accounts for the influence of defects in the light emission characteristics. The I_{EL} versus J for different emission sub-bands is plotted and shown

in the inset of Figure 8a. The exponent "*m*" value is extracted from the linear part of the log−log plot of I_{EL} versus J and is found to be 0.22, 0.53, 0.77, 0.92, and 0.81 for EL peaks centered at 422, 460, 535, 640, and 775 nm, respectively. This sublinear dependence of integrated EL intensity with injected current density can be attributed to the presence of nonradiative recombination centers in the ZnS shell and porous Si core. The stability in device operation over a wide range of temperature is very important for practical applications under harsh conditions. The fabricated SiNWs/ZnS radial heterojunction arrays have been tested for the temperature ranges from 10 to 400 K. The results are shown in Figure 8b. A gradual decrease in the EL intensity from 10 to 300 K is recorded, while above 300 K the intensity decreases rapidly. However, a significant emission observed even at 400 K indicates that as-fabricated SiNWs/ZnS heterojunction arrays could work efficiently at an elevated temperature. The results indicate the potential of lithography-free bottom-up approach for the fabrication of large-area white light emitting devices on a Si platform.

CONCLUSION

In summary, we have fabricated p-Si nanowire/n-ZnS core−shell-type radial heterojunction-based novel nanoarchitecture arrays over a large area, by combining metal-assisted chemical etching and pulsed laser deposition techniques. The anisotropic etching behavior of Si nanowire in KOH has been utilized to fabricate the isolated n-ZnS/p-Si heterojunction. The current−voltage characteristic of the fabricated radial heterojunction exhibits superior rectification behavior with high forward current and low leakage current density over the planar device. The fabricated SiNWs/ZnS radial heterojunction arrays exhibit broad emission characteristics under electrical injection, covering the full visible and NIR region up to 850 nm under low forward bias. This broad EL emission is well-explained by comparing with the PL results and proposed energy band alignment under forward bias. The white light emission from these nanoheterojunction arrays in the temperature range of 10−400 K at low applied bias indicates their potential to operate over a wide temperature range. The study demonstrates the potential of chemically etched large-area Si nanowire arrays for white light emitting devices by integrating with direct band gap II−VI semiconductors. It may be noted that a technique based on chemical vapor deposition instead of "PLD" will be more beneficial for fabricating the large-area n-ZnS/p-Si LED devices.

ASSOCIATED CONTENT

Supporting Information

Optical transmittance spectra of 20 nm thick AZO film grown on glass substrate, effect of KOH etching time on the nanowire morphologies, and temperature-dependent PL spectra of porous Si nanowires. This material is available free of charge via the Internet at http://pubs.acs.org.

AUTHOR INFORMATION

Corresponding Author

*E-mail: physkr@phy.iitkgp.ernet.in.

Notes

The authors declare no competing financial interest.

ACKNOWLEDGMENTS

We acknowledge the partial financial support from DST-sponsored "NSH" and DST-ITPAR "GPU" projects.

REFERENCES

(1) Salib, M.; Liao, L.; Jones, R.; Morse, M.; Liu, A.; Samara-Rubio, D.; Alduino, D.; Paniccia, M. Silicon Photonics. *Intel Technol. J.* **2004**, *8*, 143−160.
(2) Kimerling, L. C. Photons to the Rescue: Microelectronics Becomes Microphotonics. *Electrochem. Soc. Interface* **2000**, *9*, 28−33.
(3) Gunn, C. CMOS Photonics—SOI Learns a New Trick. Presented at the IEEE SOI Conference, Honolulu, HI, 2005; 7−13.
(4) Canham, L. T. Silicon Quantum Wire Array Fabrication by Electrochemical and Chemical Dissolution of Wafers. *Appl. Phys. Lett.* **1990**, *57*, 1046−1048.
(5) Cheng, C. H.; Lien, Y. C.; Wu, C. L.; Lin, G. R. Mutlicolor Electroluminescent Si Quantum Dots Embedded in SiOx Thin Film MOSLED with 2.4% External Quantum Efficiency. *Opt. Express* **2013**, *21*, 391−403.
(6) Das, B.; McGinnis, S. P. Porous Silicon pn Junction Light Emitting Diodes. *Semicond. Sci. Technol.* **1999**, *14*, 988−993.
(7) Xu, J.; Steckl, A. J. Stain-Etched Porous Silicon Visible Light Emitting Diodes. *J. Vac. Sci. Technol., B* **1995**, *13*, 1221−1224.
(8) Irrera, A.; Artoni, P.; Iacona, F.; Pecora, E. F.; Franzo, G.; Galli, M.; Fazio, B.; Boninelli, S.; Priolo, F. Quantum Confinement and Electroluminescence in Ultrathin Silicon Nanowires Fabricated by a Maskless Etching Technique. *Nanotechnology* **2012**, *23*, 075204.
(9) Hayden, O.; Greytak, A. B.; Bell, D. C. Core−Shell Nanowire Light-Emitting Diodes. *Adv. Mater.* **2005**, *17*, 701−704.
(10) Fabbri, F.; Rotunno, E.; Lazzarini, L.; Fukata, N.; Salviati, G. Visible and Infra-Red Light Emission in Boron-Doped Wurtzite Silicon Nanowires. *Sci. Rep.* **2013**, *4*, 3603.
(11) Velumani, S.; Ascencio, J. A. Formation of ZnS Nanorods by Simple Evaporation Technique. *Appl. Phys. A: Mater. Sci. Process.* **2004**, *79*, 153−156.
(12) Rizzo, A.; Li, Y.; Kudera, S.; Sala, F. D. Blue Light Emitting Diodes Based on Fluorescent Cd Se Zn S Nanocrystals. *Appl. Phys. Lett.* **2007**, *90*, 051106.
(13) Bae, W. K.; Kwak, J.; Lee, J. D.; Nam, M. K.; Char, K.; Lee, C.; Lee, S. Deep Blue Light-Emitting Diodes Based on Cd1−xZnxS@ZnS Quantum Dots. *Nanotechnology* **2009**, *20*, 075202.
(14) Dimitrova, V.; Tate, J. Synthesis and Characterization of Some ZnS-Based Thin Film Phosphors for Electroluminescent Device Applications. *Thin Solid Films* **2000**, *365*, 134−138.
(15) Kumbhojkar, N.; Nikesh, V. V.; Kshirsagar, A.; Mahamunia, S. Photophysical Properties of ZnS Nanoclusters. *J. Appl. Phys.* **2000**, *88*, 6260−6264.
(16) Hu, J.; Bando, Y.; Liu, Z.; Sekiguchi, T.; Golberg, D.; Zhan, J. Epitaxial Heterostructures: Side-to-Side Si-ZnS, Si-ZnSe Biaxial Nanowires, and Sandwichlike ZnS-Si-ZnS Triaxial Nanowires. *J. Am. Chem. Soc.* **2003**, *125*, 11306−11313.
(17) Xu, H. J.; Li, X. J. Structure and Photoluminescent Properties of a ZnS/Si Nanoheterostructure Based on a Silicon Nanoporous Pillar Array. *Semicond. Sci. Technol.* **2009**, *24*, 075008.
(18) Caifeng, W.; Qingshan, L.; Bo, H.; Weibing, L. White Light Photoluminescence From ZnS Films on Porous Si Substrates. *J. Semicond.* **2010**, *31*, 3.
(19) Xu, H. J.; Jia, H. S.; Yao, Z. T.; Li, X. J. Photoluminescence and I-V Characteristics of ZnS Grown on Silicon Nanoporous Pillar Array. *J. Mater. Res.* **2008**, *23*, 121−126.
(20) Dawood, M. K.; Tripathy, S.; Dolmanan, S. B.; Ng, T. H.; Tan, H. Influence of Catalytic Gold and Silver Metal Nanoparticles on Structural, optical, and Vibrational Properties of Silicon Nanowires Synthesized by Metal-Assisted Chemical Etching. *J. Appl. Phys.* **2012**, *112*, 133−138.
(21) Azeredo, B. P.; Sadhu, J.; Ma, J.; Jacobs, K.; Kim, J.; Lee, K.; Eraker, J. H.; Li, X.; Sinha, S.; Fang, N.; Ferreira, P.; Hsu, K. Silicon Nanowires With Controlled Sidewall Profile and Roughness

Fabricated by Thin-Film Dewetting and Metal-Assisted Chemical Etching. *Nanotechnology* **2013**, *24*, 225305.
(22) Zhang, M. L.; Peng, K. Q.; Fan, X.; Jie, J. S.; Zhang, R. Q.; Lee, S. T.; Wong, N. B. Preparation of Large-Area Uniform Silicon Nanowires Arrays Through Metal-Assisted Chemical Etching. *J. Phys. Chem. C* **2008**, *112*, 4444−4450.
(23) Jung, J. Y.; Guo, Z.; Jee, S.; Um, H. D.; Park, K. T.; Lee, J. H. A Strong Antireflective Solar Cell Prepared by Tapering Silicon Nanowires. *Opt. Express* **2010**, *18*, 286−292.
(24) Hung, Y. J.; Lee, S. L.; Wu, K. C.; Tai, Y.; Pan, Y. T. Antireflective Silicon Surface with Vertical Aligned Silicon Nanowires Realized by Simple Wet Chemical Etching Processes. *Opt. Express* **2011**, *19*, 15792−15802.
(25) Ye, C.; Fang, X.; Li, G.; Zhang, L. Origin of the Green Photoluminescence from Zinc Sulfide Nanobelts. *Appl. Phys. Lett.* **2004**, *85*, 3035−3037.
(26) Basu, S. *Crystalline Silicon—Properties and Uses*; InTech Publications: Rijeka, Croatia, 2011.
(27) Denzler, D.; Olschewski, M.; Sattlera, K. Luminescence Studies of Localized Gap States in Colloidal ZnS Nanocrystals. *J. Appl. Phys.* **1998**, *84*, 2841−2845.
(28) Goswami, N.; Sen, P. Photoluminescent Properties of ZnS Nanoparticles Prepared by Electro-Explosion of Zn Wires. *J. Nanopart. Res.* **2007**, *9*, 513−517.
(29) Hochbaum, A. I.; Gargas, D.; Hwang, Y. J.; Yang, P. Single Crystalline Mesoporous Silicon Nanowires. *Nano Lett.* **2009**, *9*, 3550−3554.
(30) Qu, Y.; Liao, L.; Li, Y.; Zhang, H.; Huang, Y.; Duan, X. Electrically Conductive and Optically Active Porous Silicon Nanowires. *Nano Lett.* **2009**, *9*, 4539−4543.
(31) Malinovska, D. D.; Nikolaeva, M. Transport Mechanisms and Energy Band Diagram in ZnO/Porous-Si Light-Emitting Diodes. *Vacuum* **2003**, *69*, 227−231.
(32) Islam, M. M.; Ishizuka, S.; Yamada, A.; Sakurai, K.; Niki, S.; Sakurai, T.; Akimoto, K. CIGS Solar Cell With MBE-Grown ZnS Buffer Layer. *Sol. Energy Mater. Sol. Cells* **2009**, *93*, 970−972.
(33) Zhaoa, W.; Zhaoa, L.; Shia, Z.; Xia, X.; Li, X.; Donga, X.; Changa, Y.; Zhanga, B.; Dua, G. Electroluminescence of the p-ZnO:As/n-ZnO LEDs Grown on ITO Glass Coated with GaAs Interlayer. *Appl. Surf. Sci.* **2011**, *257*, 4685−4688.
(34) Tsukazaki, A.; Kubota, M.; Oohatomo, A.; Onuma, T.; Ohatani, K.; Ohno, H.; Chichibu, S. F.; Kawasaki, M. Blue Light-Emitting Diode Based on ZnO. *Jpn. J. Appl. Phys.* **2005**, *44*, 643−645.
(35) Wang, C. F.; Li, Q. S.; Lv, L.; Zhang, L. C.; Qi, H. X.; Chen, H. Structural, Optical and Electrical Properties of ZnS Porous Si Heterostructures. *Chin. Phys. Lett.* **2007**, *24*, 825−827.
(36) Jian, H.; Lin, J. W.; Ke, T.; Ru, X.; Ji, J. Z.; Xiong, G. L.; Yi, B. X. Photoresponse Properties of an n-ZnS/p-Si Heterojunction. *Chin. Phys. Lett.* **2011**, *28*, 127301.